Vector theory of diffraction by gratings made of a uniaxial dielectric–magnetic material exhibiting negative refraction

Ricardo A. Depine and Marina E. Inchaussandague

Grupo de Electromagnetismo Aplicado, Departamento de Física, Facultad de Ciencias Exactas y Naturales, Universidad de Buenos Aires, Ciudad Universitaria, Pabellón I, 1428 Buenos Aires, Argentina, and Consejo Nacional de Investigaciones Científicas y Técnicas, Rivadavia 1917, Buenos Aires, Argentina

Akhlesh Lakhtakia

Computational and Theoretical Materials Sciences Group, Department of Engineering Science and Mechanics, Pennsylvania State University, University Park, Pennsylvania 16802-6812, and Department of Physics, Imperial College, London SW7 2AZ, UK

Received July 8, 2005; accepted August 25, 2005; posted September 23, 2005 (Doc. ID 63300)

Diffraction of linearly polarized plane electromagnetic waves at the periodically corrugated boundary of vacuum and a linear, homogeneous, nondissipative, uniaxial dielectric–magnetic material is formulated as a boundary-value problem and solved using the differential method. Attention is paid to two classes of diffracting materials: those with negative definite permittivity and permeability tensors and those with indefinite permittivity and permeability tensors. The dispersion equations turn out to be elliptic for the first class of diffracting materials, whereas for the second class they can be hyperbolic, elliptic, or linear, depending on the orientation of the optic axis. When the dispersion equations are elliptic, the optical response of the grating is qualitatively similar to that for conventional gratings: a finite number of refraction channels are supported. On the other hand, hyperbolic or linear dispersion equations imply the possibility of an infinite number of refraction channels. This possibility seriously incapacitates the differential method as the corrugations deepen. © 2006 Optical Society of America

OCIS codes: 050.1950, 160.1190.

1. INTRODUCTION

During the past five years, much research has been reported on the electromagnetic responses of negatively refracting, isotropic dielectric–magnetic materials.[1–3] Materials with these constitutive properties are characterized by a negative index of refraction because the phase velocity vector is in the opposite direction of the energy flux. As McCall *et al.*[4] and Boardman *et al.*[5] have pointed out, it is best to call these materials negative-phase-velocity (NPV) materials. Of late, focus is shifting to anisotropic materials wherein the phase velocity vector is not necessarily antiparallel to the time-averaged Poynting vector but—more generally—casts a negative projection thereupon.[6] This is because the NPV materials synthesized thus far are actually anisotropic in nature, and any hypothesis about their isotropic behavior holds only under some restrictions on propagation direction and polarization state. Furthermore, the use of anisotropic NPV materials offers flexibility in design and ease of fabrication.[7–11]

An important device in optics is the surface-relief grating.[12] Therefore, last year we began to investigate diffraction of plane waves by gratings made of isotropic NPV materials.[13–15] We were motivated by two reasons. First, NPV materials promise new types of grating that could be significantly different from those made with their positive-phase-velocity (PPV) counterparts. Second, all experimental realizations of NPV materials thus far are as periodically patterned composite materials, with the unit-cell size smaller, although not extremely, than the wavelength. Owing to this finite electrical size of the unit cell, the exposed surface of a NPV material is not specularly planar but periodically modulated instead.[16,17] We found that—when the boundary between vacuum and a isotropic, homogeneous dielectric–magnetic material is periodically corrugated—the replacement of a NPV diffracting material by its PPV analog affects mainly the nonspecular reflectances and refractances when the corrugations are shallow and that the effect on the specular reflectance and refractance intensifies as the corrugations deepen.

We went on to compute diffraction by gratings made of a uniaxial dielectric–magnetic material under the condition that the polarization states of the incident plane wave and of the reflected and the refracted Floquet harmonics are identical and either s or p polarized.[18] We adapted the Rayleigh method for this purpose and ignored dissipation in the diffracting material. Under certain conditions fulfilled by the constitutive properties of the diffracting material, such gratings were found to support an infinite number of refracted Floquet harmonics; it was also found that in these cases the Rayleigh method either lacked good convergence or completely failed, even within the expected validity range of the Rayleigh hypothesis. More recently, with a scalar version of the dif-

ferential method of Chandezon *et al.* and other researchers[19–23]—also called the differential method and the C method—this lack of convergence was shown to be related to the existence of an infinite number of refraction channels and not to be exclusive to the Rayleigh method.[24]

In this paper, we extend our consideration to the general case when the polarization states of the reflected and the refracted Floquet harmonics can be different from the polarization state of the incident plane wave (which is still taken to be linear). Four constitutive scalars are needed to characterize the diffracting material: $\epsilon_{\parallel}$ and $\mu_{\parallel}$, which are the respective elements of the relative permittivity and relative permeability tensors along the optics axis, and $\epsilon_{\perp}$ and $\mu_{\perp}$, which are the elements of the two tensors in the plane perpendicular to the optic axis. These scalars have positive real parts for natural crystals, but their real parts can have any sign for artificial (but still effectively homogeneous) materials. The dispersion equation for plane waves in such a material can be factorized into two terms, leading to the conclusion that the material supports the propagation of two different types of linearly polarized wave, called magnetic and electric modes.[25,26] The geometric representation of these dispersion equations in the wave-vector space depends on certain relevant properties of the relative permittivity and the relative permeability tensors and may take unusual forms, compared with the case of natural crystals.[27]

As the relative permittivity and permeability tensors of the (nondissipative) diffracting material are real symmetric, each can be classified as (i) positive definite, (ii) negative definite, or (iii) indefinite.[28] If all eigenvalues of a real symmetric tensor are >0, it is positive definite; if all eigenvalues are <0, it is negative definite; but if it has both negative and positive eigenvalues, then it is indefinite. Thus, the relative permittivity tensor is positive definite if $\epsilon_{\perp}>0$ and $\epsilon_{\parallel}>0$; it is negative definite if $\epsilon_{\perp}<0$ and $\epsilon_{\parallel}<0$; and it is indefinite if $\epsilon_{\perp}\epsilon_{\parallel}<0$. A similar classification applies to the relative permeability tensor. If both $\tilde{\epsilon}$ and $\tilde{\mu}$ are positive definite, the material is of the PPV kind. We have recently shown[27] that, depending on the combination of permittivity and permeability tensors, magnetic and electric propagating modes can exhibit dispersion surfaces in the form of (a) ellipsoids of revolution, (b) one-sheet hyperboloids, or (c) two-sheet hyperboloids. Thus, depending on the relative orientation of the optic axis, circles, ellipses, hyperbolas, or straight lines can be obtained as a result of the intersection between these surfaces and a fixed plane of propagation.

The plan of this paper is as follows. Section 2 contains a description of the boundary-value problem for the diffraction of a plane wave by a surface-relief grating made of the chosen anisotropic NPV material, and the description of the differential method adopted to solve the problem numerically is presented in Section 3. Section 4 is devoted to a discussion of numerical results for two important classes of the diffracting material: either both the relative permittivity and the relative permeability tensors are negative definite (Subsection 4.A) or both are indefinite (Subsection 4.B). The case of deep gratings is considered in Subsection 4.C. Concluding remarks are provided in Section 5. An $\exp(-i\omega t)$ time dependence is implicit, with ω as angular frequency, t as time, and $i=\sqrt{-1}$. A Cartesian coordinate system $Oxyz$ is used, such that the x and z axis are perpendicular and parallel, respectively, to the grating grooves.

2. BOUNDARY-VALUE PROBLEM

Let us consider the diffraction of a plane wave at a periodically corrugated boundary between vacuum and a linear, homogeneous, nondissipative, uniaxial dielectric–magnetic medium. The relative permittivity and permeability tensors of the diffracting medium share the same optic axis denoted by the unit vector $\hat{c}$, and their four eigenvalues are denoted by $\epsilon_{\perp,\parallel}$ and $\mu_{\perp,\parallel}$; thus,

$$\tilde{\epsilon}=\epsilon_{\perp}\tilde{I}+(\epsilon_{\parallel}-\epsilon_{\perp})\hat{c}\hat{c},$$

$$\tilde{\mu}=\mu_{\perp}\tilde{I}+(\mu_{\parallel}-\mu_{\perp})\hat{c}\hat{c}, \tag{1}$$

in dyadic notation with $\tilde{I}$ as the identity dyadic.[29] The orientation of the optic axis

$$\hat{c}=\hat{x}\sin\theta_c\cos\phi_c+\hat{y}\cos\theta_c+\hat{z}\sin\theta_c\sin\phi_c \tag{2}$$

is given by the spherical angles θ_c, the angle between the optic axis and the y axis, and ϕ_c, the angle between the x axis and the projection of the optic axis onto the xz plane; see Fig. 1.

The grating surface described by the periodic function $y=a(x)=a(x\pm d)$ is illuminated from the vacuous half-space $[y>a(x)]$ by either an s- or a p-polarized plane wave, with its wave vector $\vec{k}_i$ lying on the mean section of the grating (xy plane) and forming an angle θ_0 with the y axis; i.e.,

$$\vec{k}_i=\alpha_0\hat{x}-\beta_0\hat{y},$$

$$\alpha_0=k_0\sin\theta_0,$$

$$\beta_0=k_0\cos\theta_0, \tag{3}$$

where k_0 denotes the vacuum wavenumber.

In the region $y>\max a(x)$, the electromagnetic fields are rigorously represented by the following Floquet expansions:

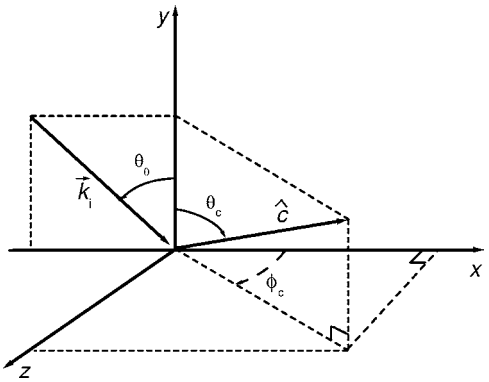

Fig. 1. Schematic for the incident wave vector $\vec{k}_i$ and the optic axis of the diffracting medium.

$$\vec{E}_1 = \left[A^{(p)} \left(\frac{\beta_0^{(1)}}{k_0} \hat{x} + \frac{\alpha_0}{k_0} \hat{y} \right) + A^{(s)} \hat{z} \right] \exp[i(\alpha_0 x - \beta_0^{(1)} y)] + \sum_{n=-\infty}^{+\infty} \left[R_n^{(p)} \left(-\frac{\beta_n^{(1)}}{k_0} \hat{x} + \frac{\alpha_n}{k_0} \hat{y} \right) + R_n^{(s)} \hat{z} \right] \exp[i(\alpha_n x + \beta_n^{(1)} y)], \tag{4}$$

$$\vec{H}_1 = \left[A^{(s)} \left(-\frac{\beta_0^{(1)}}{k_0} \hat{x} + \frac{\alpha_0}{k_0} \hat{y} \right) + A^{(p)} \hat{z} \right] \exp[i(\alpha_0 x - \beta_0^{(1)} y)] + \sum_{n=-\infty}^{+\infty} \left[R_n^{(s)} \left(\frac{\beta_n^{(1)}}{k_0} \hat{x} - \frac{\alpha_n}{k_0} \hat{y} \right) + R_n^{(p)} \hat{z} \right] \exp[i(\alpha_n x + \beta_n^{(1)} y)]. \tag{5}$$

In the foregoing expressions, $A^{(s)}$ and $A^{(p)}$ are complex-valued amplitudes that define the polarization state of the incident plane wave; $R_n^{(s)}$ and $R_n^{(p)}$ are unknown complex-valued amplitudes of the reflected Floquet harmonics; and

$$\alpha_n = \alpha_0 + 2\pi n/d,$$

$$\beta_n^{(1)} = +(k_0^2 - \alpha_n^2)^{1/2}. \tag{6}$$

In the diffracting medium, the total fields in the region below the corrugations $[y < \min a(x)]$ can also be rigorously represented by Floquet expansions, now in terms of electric-type (superscript E) and magnetic-type (superscript M) plane waves, as follows:

$$\vec{E}_2 = \sum_{n=-\infty}^{+\infty} [C_n^{(E)} \vec{e}_n^{(E)} \exp(i\vec{k}_n^{(E)} \cdot \vec{r}) + C_n^{(M)} \vec{e}_n^{(M)} \exp(i\vec{k}_n^{(M)} \cdot \vec{r})], \tag{7}$$

$$\vec{H}_2 = \sum_{n=-\infty}^{+\infty} [C_n^{(E)} \vec{h}_n^{(E)} \exp(i\vec{k}_n^{(E)} \cdot \vec{r}) + C_n^{(M)} \vec{h}_n^{(M)} \exp(i\vec{k}_n^{(M)} \cdot \vec{r})]. \tag{8}$$

In these expressions $\vec{k}_n^{(l)} = \alpha_n \hat{x} + \beta_n^{(l)} \hat{y}$ $(l = E, M)$ are the wave vectors associated with the Floquet harmonics of the electric and magnetic types. These wave vectors are found as solutions satisfying the radiation condition as $y \to -\infty$ of the dispersion equations[29]

$$\vec{k}_n^{(E)} \cdot \vec{\epsilon} \cdot \vec{k}_n^{(E)} = k_0^2 \mu_\perp \epsilon_\perp \epsilon_\parallel, \tag{9}$$

for Floquet harmonics of the electric type, and for the magnetic Floquet harmonics we have

$$\vec{k}_n^{(M)} \cdot \tilde{\mu} \cdot \vec{k}_n^{(M)} = k_0^2 \mu_\perp \epsilon_\perp \mu_\parallel. \tag{10}$$

The vectors $\vec{e}_n^{(l)}$ $(l = E, M)$ specify the polarization state of the electric field associated with the electric and magnetic Floquet harmonics, and the vectors $\vec{h}_n^{(l)}$ $(l = E, M)$ are related to $\vec{e}_n^{(l)}$ according to the time-harmonic Maxwell equations. The unknown complex-valued amplitudes of the refracted Floquet harmonics are denoted by $C_n^{(E)}$ and $C_n^{(M)}$.

3. DIFFERENTIAL METHOD

Let us now briefly outline the main steps of the differential method for the chosen gratings, following closely the notation used by Li[20] for anisotropic dielectric gratings. First, to encompass gratings whose profiles are overhanging or have a vertical or almost vertical facet, we introduce an oblique Cartesian coordinate system $(O\bar{x}^1\bar{x}^2\bar{x}^3)$ as

$$\bar{x}^1 = x - y \tan\zeta,$$

$$\bar{x}^2 = y \sec\zeta,$$

$$\bar{x}^3 = z, \tag{11}$$

where the directions of the $\bar{x}^1$ and the x axes coincide and ζ is the angle between the $\bar{x}^2$ and the y axes. Second, another coordinate system $(Ox^1x^2x^3)$ is then defined by

$$x^1 = \bar{x}^1,$$

$$x^2 = \bar{x}^2 - a(\bar{x}^1),$$

$$x^3 = \bar{x}^3. \tag{12}$$

Under the transformations (11) and (12), the periodically corrugated boundary is transformed into a plane, thus simplifying the treatment of the boundary conditions but requiring us to express the time-harmonic Maxwell equations in the transformed coordinates as follows[20]:

$$\xi^{\rho\sigma\tau} \partial_\sigma H_\tau = -ik_0 \sqrt{g}\, \epsilon^{\rho\sigma} E_\sigma, \tag{13}$$

$$\xi^{\rho\sigma\tau} \partial_\sigma E_\tau = ik_0 \sqrt{g}\, \mu^{\rho\sigma} H_\sigma. \tag{14}$$

Here, $\partial_\sigma \equiv \partial/\partial x^\sigma$, $g = [\mathrm{Det}(g^{\rho\sigma})]^{-1}$ and $g^{\rho\sigma}$ is the contravariant metric tensor, $\xi^{\rho\sigma\tau}$ is the permutation tensor of rank three,[30] and the summation convention applies. The quantities $\epsilon^{\rho\sigma}$ and $\mu^{\rho\sigma}$ are the components of the tensors $\tilde{\epsilon}$ and $\tilde{\mu}$ in the coordinate system $Ox^1x^2x^3$, obtained by the tensor transformation rules.

The essence of the differential method is the solution of the Maxwell equations (13) and (14) by transforming them into a matrix eigenvalue problem in Fourier space. The electric and magnetic fields are expanded as the Floquet–Fourier series

$$E_\sigma(x^1, x^2) = \sum_n E_{\sigma n}(x^2) \exp(i\alpha_n x^1), \tag{15}$$

$$H_\sigma(x^1, x^2) = \sum_n H_{\sigma n}(x^2) \exp(i\alpha_n x^1), \tag{16}$$

which are then substituted into Eqs. (13) and (14). However, the Fourier series of $\epsilon^{\rho\sigma}$ and $\mu^{\rho\sigma}$ cannot be substituted directly because that step slows down numerical convergence when grating profiles have sharp edges. To avoid this problem, one can exploit the theory of Fourier factorization. We refer the reader to Li[20] for details on this point—basically, the procedure consists of finding the Fourier factorization of $D^\rho = \epsilon^{\rho\sigma} E_\sigma$ and $B^\rho = \mu^{\rho\sigma} H_\sigma$. Thereafter, the Fourier analogs of Eqs. (13) and (14) are obtained as

$$(\xi^{\rho\sigma\tau}\partial_\sigma H_\tau)_m = -ik_0\sqrt{g}\sum_n (\mathsf{e}^{\rho\sigma})_{mn}E_{\sigma n}, \tag{17}$$

$$(\xi^{\rho\sigma\tau}\partial_\sigma E_\tau)_m = ik_0\sqrt{g}\sum_n (\mathsf{m}^{\rho\sigma})_{mn}H_{\sigma n}, \tag{18}$$

where $\mathsf{e}^{\rho\sigma}$ and $\mathsf{m}^{\rho\sigma}$ are now submatrices of the 3×3 block matrices e and m, respectively, as provided in Appendix A.

If the medium is isotropic, then $\epsilon^{\rho\sigma}=\epsilon g^{\rho\sigma}$ and $\mu^{\rho\sigma}=\mu g^{\rho\sigma}$. Accordingly, Eqs. (17) and (18) can be greatly simplified, leading to

$$(\xi^{\rho\sigma\tau}\partial_\sigma H_\tau)_m = -ik_0\sqrt{g}\epsilon\sum_n (G^{\rho\sigma})_{mn}E_{\sigma n}, \tag{19}$$

$$(\xi^{\rho\sigma\tau}\partial_\sigma E_\tau)_m = ik_0\sqrt{g}\mu\sum_n (G^{\rho\sigma})_{mn}H_{\sigma n}, \tag{20}$$

where $G^{\rho\sigma}$ is also given in Appendix A.

Once the Fourier analysis is complete, the derivation of the eigenvalue problem is straightforward. In the vacuous region, with either $F=E$ or $F=H$, we have

$$-i\partial_2\begin{pmatrix}F_3\\ F_3'\end{pmatrix} = \begin{bmatrix}0 & 1\\ (G^{22})^{-1}\Gamma^2 & -(G^{22})^{-1}(\boldsymbol{\alpha}G^{12}+G^{21}\boldsymbol{\alpha})\end{bmatrix}\begin{pmatrix}F_3\\ F_3'\end{pmatrix}, \tag{21}$$

where $\boldsymbol{\alpha}$ is a diagonal matrix with diagonal elements α_m, $F_3'=-i\partial_2 F_3$, and the matrix Γ^2 is defined as $\Gamma^2=k_0^2\tilde{I}-g^{11}\boldsymbol{\alpha}^2$. In the diffracting medium, the corresponding equation is

$$-i\partial_2\begin{pmatrix}E_3\\ H_3\\ H_1\\ E_1\end{pmatrix} = \begin{bmatrix}-T_{12}\boldsymbol{\alpha} & \kappa_0 T_{13} & \kappa_0 T_{11} & 0\\ -\kappa_0 Z_{13} & -Z_{12}\boldsymbol{\alpha} & 0 & -\kappa_0 Z_{11}\\ -\boldsymbol{\alpha}T_{22}\boldsymbol{\alpha}+\kappa_0 Z_{33} & -\boldsymbol{\alpha}T_{23}+Z_{32}\boldsymbol{\alpha} & -\boldsymbol{\alpha}T_{21} & \kappa_0 Z_{31}\\ -\boldsymbol{\alpha}Z_{23}+T_{32}\boldsymbol{\alpha} & \boldsymbol{\alpha}Z_{22}\boldsymbol{\alpha}-\kappa_0 T_{33} & -\kappa_0 T_{31} & -\boldsymbol{\alpha}Z_{21}\end{bmatrix}\begin{pmatrix}E_3\\ H_3\\ H_1\\ E_1\end{pmatrix}, \tag{22}$$

where $\kappa_0=k_0\cos\zeta$ and $Z_{\rho\sigma}$ and $T_{\rho\sigma}$ are matrices provided in Appendix B.

Since the matrices on the right side of expressions (21) and (22) do not depend on x^2, the search for solutions leads to the prescription of an eigenvalue problem in each region:

$$\mathsf{A}\mathsf{x} = \lambda\mathsf{x}. \tag{23}$$

Here A and x are the matrix and the column vector in Eq. (21) for the vacuous region and in expression (22) for the diffracting medium, whereas λ denotes the eigenvalue.

The next step is to write the total fields in regions $y>a(x)$ and $y<a(x)$. In the vacuous side, the total field can be written as a superposition of the incident wave and all the eigensolutions that correspond to positive real eigenvalues or to complex eigenvalues with positive imaginary parts. In practice, we replace the real eigensolutions with their Rayleigh counterparts. Thus, we write the z component of the the total field as

$$F_3 = A^{(f)}\exp[i(\alpha_0\bar{x}^1+\tilde{\beta}_0^{(1)-}\bar{x}^2)] + \sum_{n\in U^+} R_n^{(f)}\exp[i(\alpha_n\bar{x}^1 + \tilde{\beta}_n^{(1)+}\bar{x}^2)] + \sum_m \exp(i\alpha_m x^1)\sum_{q\in V^+} F_{3mq}\exp(i\lambda_q^+ x^2)u_q^{(f)}, \tag{24}$$

where $f=s$ or p when $F=E$ or H; U^+ are the sets of integers n for which $\tilde{\beta}_n^{(1)+}$ are real and V^+ are the sets of integers q such that the eigenvalues λ_q^+ of Eq. (21) have positive imaginary parts; $A^{(f)}$ and $R_n^{(f)}$ are the incident and diffracted amplitudes; and $\tilde{\beta}_n^{(1)\pm}=\alpha_n\sin\zeta\pm\beta_n^{(1)}\cos\zeta$.

The total field in the diffracting medium is given by

$$\mathbf{F} = \sum_{l=E,M}\sum_{n\in U_l^-}\mathbf{f}_n^{(l)}\exp[i(\alpha_n\bar{x}^1+\tilde{\beta}_{ln}\bar{x}^2)]C_n^{(l)} + \mathbf{b}^\sigma\sum_m\sum_{q\in V^-}F_{\sigma mq}\exp[i(\alpha_m x^1+\lambda_q^- x^2)]d_q. \tag{25}$$

Here, U_l^- and V^- are the sets of integers that, respectively, represent the downward propagating Rayleigh waves and the downward evanescent eigensolutions of the eigenvalue problem in the diffracting medium, $C_n^{(l)}$ and d_q are the corresponding unknown field amplitudes, and $\mathbf{b}^\sigma$ are the contravariant basis vectors of the system $Ox^1x^2x^3$. Because it is possible that only one of the two downward waves is propagating (electric or magnetic), the sets U_l^- depend on the subscript l. The vectors $\mathbf{f}_n^{(l)}$ are equal either to $\mathbf{e}$ or $\mathbf{h}$ and are determined in the coordinate system $Oxyz$. The eigenvalues $\tilde{\beta}_{ln}$ are in the coordinate system $O\bar{x}^1\bar{x}^2\bar{x}^3$ and are related to the eigenvalues $\beta_n^{(l)}$ in system $Oxyz$ via the tensor transformation rules as $\tilde{\beta}_{ln}=\alpha_n\sin\zeta+\beta_n^{(l)}\cos\zeta$.

Having found the general forms of the total electromagnetic fields everywhere, we can obtain the unknown complex-valued amplitudes by matching the boundary conditions at the interface.

After the determination of the Floquet expansion coefficients, the diffraction efficiencies[31] for the propagating plane-wave components of the reflected or refracted fields

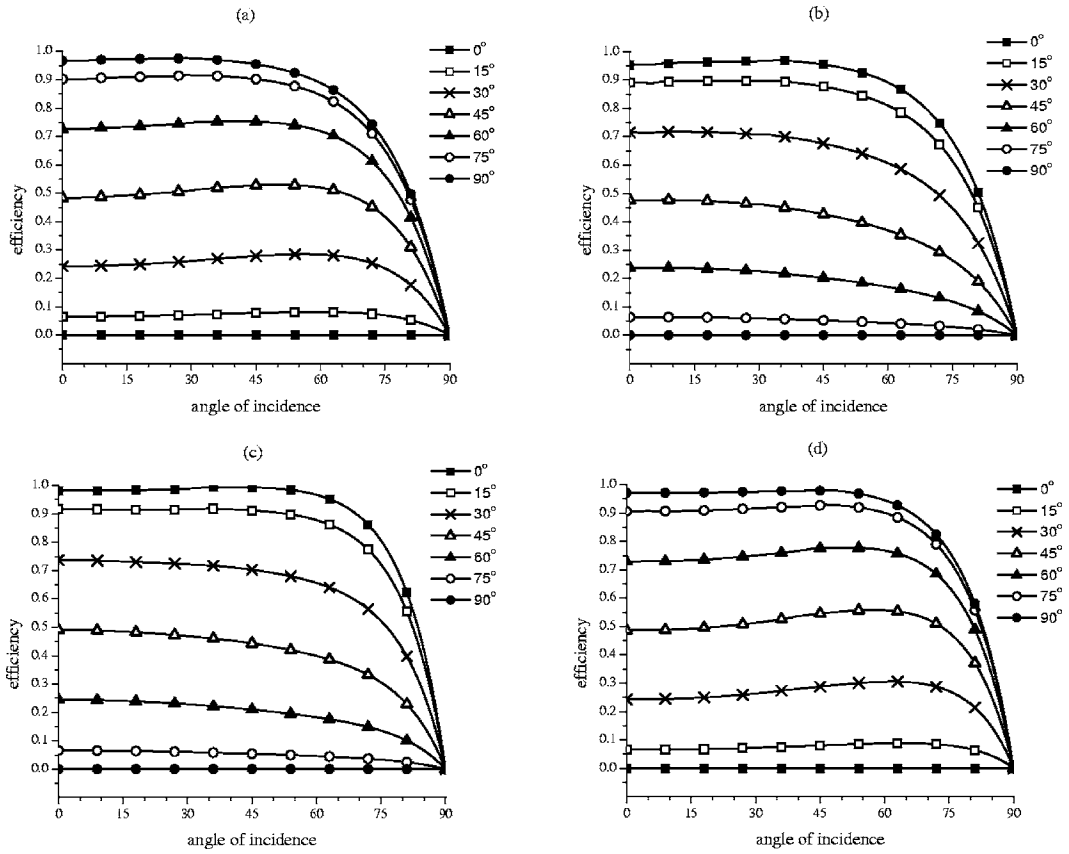

Fig. 2. Specular refraction efficiencies versus the angle of incidence θ_0 for a sinusoidal grating delineated by Eq. (29) with $h/d=0.1$ and illuminated from the vacuous region, when the constitutive scalars are chosen for case IP, $\lambda_0=1.1d$, and $\theta_c=90°$. The values of ϕ_c are indicated on the plots. (a) τ_0^{Es}, (b) τ_0^{Ms}, (c) τ_0^{Ep}, and (d) τ_0^{Mp}.

can be calculated as ratios between the diffracted and the incident intensities. These diffraction efficiencies are defined as

$$\rho_n^{ls} = \left. \frac{\mathrm{Re}[\beta_n^{(1)}]\ |R_n^l|^2}{\beta_0^{(1)}\ |A^{(s)}|^2} \right|_{A^{(p)}=0},$$

$$\rho_n^{lp} = \left. \frac{\mathrm{Re}[\beta_n^{(1)}]\ |R_n^l|^2}{\beta_0^{(1)}\ |A^{(p)}|^2} \right|_{A^{(s)}=0} \qquad (l=s,p), \tag{26}$$

for the reflected Floquet harmonics of order n. Likewise, for the refracted harmonics we have

$$\tau_n^{ls} = -\left. \frac{|C_n^{(l)}|^2}{|A^{(s)}|^2} \frac{k_0}{\beta_0^{(1)}} \mathrm{Re}\{[\vec{e}_n^{(l)} \times (\vec{h}_n^{(l)})^*] \cdot \hat{y}\} \right|_{A^{(p)}=0} \qquad (l=E,M), \tag{27}$$

$$\tau_n^{lp} = -\left. \frac{|C_n^{(l)}|^2}{|A^{(p)}|^2} \frac{k_0}{\beta_0^{(1)}} \mathrm{Re}\{[\vec{e}_n^{(l)} \times (\vec{h}_n^{(l)})^*] \cdot \hat{y}\} \right|_{A^{(s)}=0} \qquad (l=E,M), \tag{28}$$

with the asterisk denoting the complex conjugate and Re meaning the real part.

4. NUMERICAL RESULTS AND DISCUSSION

We applied the described differential method to investigate grating configurations with different characteristics of the permeability and the permittivity tensors. Basically, we considered cases in which these tensors are positive definite ($\epsilon_{\perp,\parallel}>0$ $\mu_{\perp,\parallel}>0$), negative definite ($\epsilon_{\perp,\parallel}<0$ and $\mu_{\perp,\parallel}<0$), and indefinite ($\epsilon_\perp\epsilon_\parallel<0$ and $\mu_\perp\mu_\parallel<0$).

For the sake of illustration, we present results for the following four sets of constitutive parameters:

- Case IP, positive definite constitutive tensors: $\epsilon_\perp=2.1$, $\epsilon_\parallel=1.9$, $\mu_\perp=1.3$, and $\mu_\parallel=1.6$.
- Case IN, negative definite constitutive tensors: $\epsilon_\perp=-2.1$, $\epsilon_\parallel=-1.9$, $\mu_\perp=-1.3$, and $\mu_\parallel=-1.6$.
- Case IIA, indefinite constitutive tensors: $\epsilon_\perp=-2.1$, $\epsilon_\parallel=1.9$, $\mu_\perp=1.3$, and $\mu_\parallel=-1.6$.
- Case IIB, indefinite constitutive tensors: $\epsilon_\perp=2.1$, $\epsilon_\parallel=-1.9$, $\mu_\perp=-1.3$, and $\mu_\parallel=1.6$.

For cases IP and IN (both constitutive tensors either positive or negative definite), both of the dispersion surfaces for the propagating refracted harmonics are ellipsoids of revolution, as in natural crystals. Depending on the orientation of the optic axis, the intersections between these surfaces and fixed planes of propagation are either circles or ellipses. For cases IIA and IIB (indefinite constitutive tensors), the dispersion surfaces for the propagating refracted harmonics are one-sheet hyperboloids of

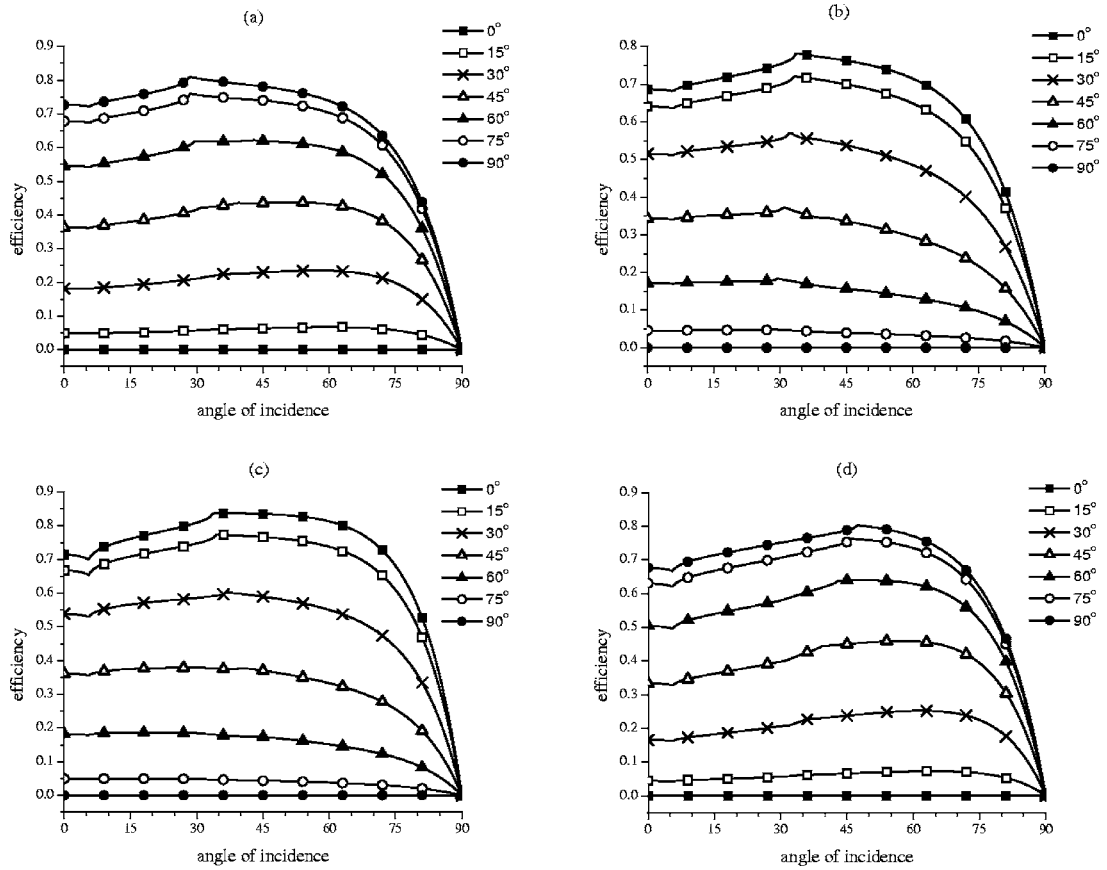

Fig. 3. Same as Fig. 2, but for case IN.

revolution whose intersections with the fixed planes of propagation are circles, ellipses, hyperbolas, or straight lines—depending on the orientation of $\hat{c}$.[27]

A. Optic Axis in the *xz* Plane

We chose the sinusoidal grating profile

$$a(x) = \frac{h}{2}\cos\left(\frac{2\pi x}{d}\right) \tag{29}$$

and set $\theta_c = 90°$ in Eq. (2). Accordingly, Eq. (9) gives the following dispersion equation for the refracted Floquet harmonics of the electric type:

$$\left(\frac{\epsilon_\parallel}{\epsilon_\perp}\cos^2\phi_c + \sin^2\phi_c\right)\alpha_n^2 + (\beta_n^{(E)})^2 = k_0^2\epsilon_\parallel\mu_\perp. \tag{30}$$

The analogous equation for modes of the refracted Floquet harmonics of the magnetic type from Eq. (10) is

$$\left(\frac{\mu_\parallel}{\mu_\perp}\cos^2\phi_c + \sin^2\phi_c\right)\alpha_n^2 + (\beta_n^{(M)})^2 = k_0^2\mu_\parallel\epsilon_\perp. \tag{31}$$

Let us start with cases IP and IN, both characterized by elliptic dispersion equations. Specular refraction efficiencies against the angle of incidence θ_0 for both cases are plotted in Figs. 2 and 3, for incident *s*- and *p*-polarization states, when $\lambda_0/d = 1.1$ and $h/d = 0.1$. Curves for seven different values of ϕ_c are presented in these figures. In Fig. 2, we observe that the zeroth refracted harmonics of both electric and magnetic types together carry almost all the energy incident onto the grating, except for near-grazing incidence angles for which specular reflection is highly intense. This behavior is observed for all orientations of the optic axis.

However, although for a flat boundary the (specular) refraction efficiencies for cases IP and IN are identical,[32] differences appear in the diffraction efficiency plots for $h/d > 0$, as can be appreciated by comparing Figs. 2 and 3. Whereas $\tau_{-1}^{\ell\ell'}$ ($\ell = E, M$; $\ell' = s, p$) are negligibly small for case IP (and therefore not presented), these are not negligible for case IN—as may be gathered from Fig. 4. Thus, as expected, all refraction efficiencies are affected by the type of diffracting medium.

Weak Rayleigh–Wood anomalies[12] manifested as discontinuities in the curves can be observed at those angles of incidence at which a refracted harmonic propagates parallel to the interface, for example, at $\theta_0 = 28.14°$ ($\phi_c = 90°$), $\theta_0 = 28.47°$ ($\phi_c = 75°$), and $\theta_0 = 29.38°$ ($\phi_c = 60°$) at which the refracted Floquet harmonic of the electric type and order $n = 1$ changes from being propagating to evanescent or at $\theta_0 = 43.03°$ ($\phi_c = 60°$), $\theta_0 = 39.47°$ ($\phi_c = 45°$), and $\theta_0 = 36.33°$ ($\phi_c = 30°$) at which the refracted Floquet harmonic of the magnetic type and order $n = 1$ changes similarly.

Let us now go on to cases IIA and IIB. As we have already mentioned, the dispersion equations for these cases can be hyperbolic or elliptic, depending on the value of ϕ_c. From Eqs. (30) and (31), we can deduce that, starting

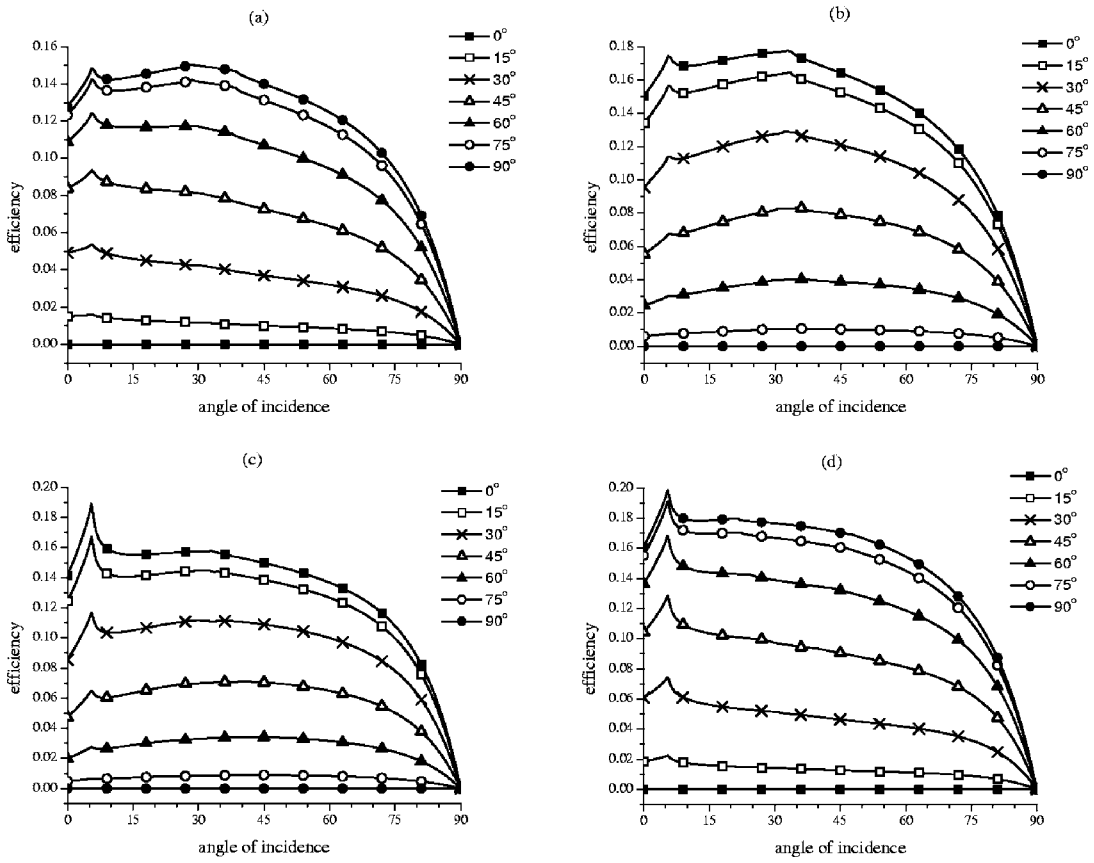

Fig. 4. Nonspecular refraction efficiencies versus the angle of incidence θ_0 for a sinusoidal grating delineated by Eq. (29) with $h/d=0.1$ and illuminated from the vacuous region, when the constitutive scalars are chosen for case IN, $\lambda_0=1.1d$, and $\theta_c=90°$. The values of ϕ_c are indicated on the plots. (a) τ_{-1}^{Es}, (b) τ_{-1}^{Ms}, (c) τ_{-1}^{Ep}, and (d) τ_{-1}^{Mp}. In contrast, these nonspecular efficiencies are negligible for case IP.

from $\phi_c=0°$, there is a critical angle at which the dispersion curves change from hyperbolic to elliptic. For refracted harmonics of the electric type, this angle is

$$\phi_c^e=\tan^{-1}[(-\epsilon_\parallel/\epsilon_\perp)^{1/2}], \tag{32}$$

whereas for the refracted harmonics of the magnetic type, the critical angle is given by

$$\phi_c^m=\tan^{-1}[(-\mu_\parallel/\mu_\perp)^{1/2}]. \tag{33}$$

When $\phi_c=\phi_c^e$, the dispersion curves for refracted Floquet harmonics propagating in the xy plane are straight lines (electric type) and hyperbolas (magnetic type), whereas, for $\phi_c=\phi_c^m$, the dispersion curves are ellipses (electric type) and straight lines (magnetic type).

Figure 5 contains the reciprocal space maps for cases IIA and IIB for four orientations of the optic axis: $\phi_c=30°$ (both dispersion curves are hyperbolic), $\phi_c=\phi_c^e=43.57°$ (electric type is linear and magnetic type is hyperbolic), $\phi_c=45°$ (electric type is elliptic and magnetic type is hyperbolic), and $\phi_c=\phi_c^m=47.97°$ (electric type is elliptic and magnetic type is linear). For $\phi_c>\phi_c^m=47.97°$, the refracted Floquet harmonics of both types have elliptic dispersion relations (not shown).

The graphical construction to find the wave vectors for the refracted Floquet harmonics is indicated in Fig. 5. The light gray circles represent the dispersion equation for plane waves in the medium of incidence, and the horizontal, light-gray double arrows represent the quantity $2\pi/d$. Note that one obtains the value of α_n by adding or subtracting an integer number times $2\pi/d$ from the x component of the incident wave vector. In Fig. 5(a) we observe that—in contrast to what happens for all gratings made of conventional materials (for which the dispersion equation for the Floquet harmonics has real-valued solutions only in a limited n range)—the dispersion equations for refracted Floquet harmonics of electric and magnetic types give real-valued solutions for all values of n. For example, for $n=1$ and harmonics of the electric type, we can find two wave vectors with real-valued components whose x components equal α_1, one belonging to the upper hyperbola and the other to the lower hyperbola. The ray directions (that is, the direction of the time-averaged Poynting vector) associated with these wave vectors are perpendicular to the hyperbolas. Significantly, wave vectors in the upper hyperbola do not satisfy the radiation condition in case IIA, whereas wave vectors in the lower hyperbola do not satisfy the radiation condition in case IIB. Thus, wave vectors and ray directions for harmonics of the electric type have y components with the same sign for case IIA, whereas they are counterposed[33] for case IIB. For magnetic modes, wave vectors and ray directions are counterposed for case IIA, whereas they have y components with the same sign for case IIB.

The refracted wave vectors $\vec{k}_n^{(E)}$ for $n=0$ and 2 are also shown in Fig. 5(a) for case IIA. Repeating the construc-

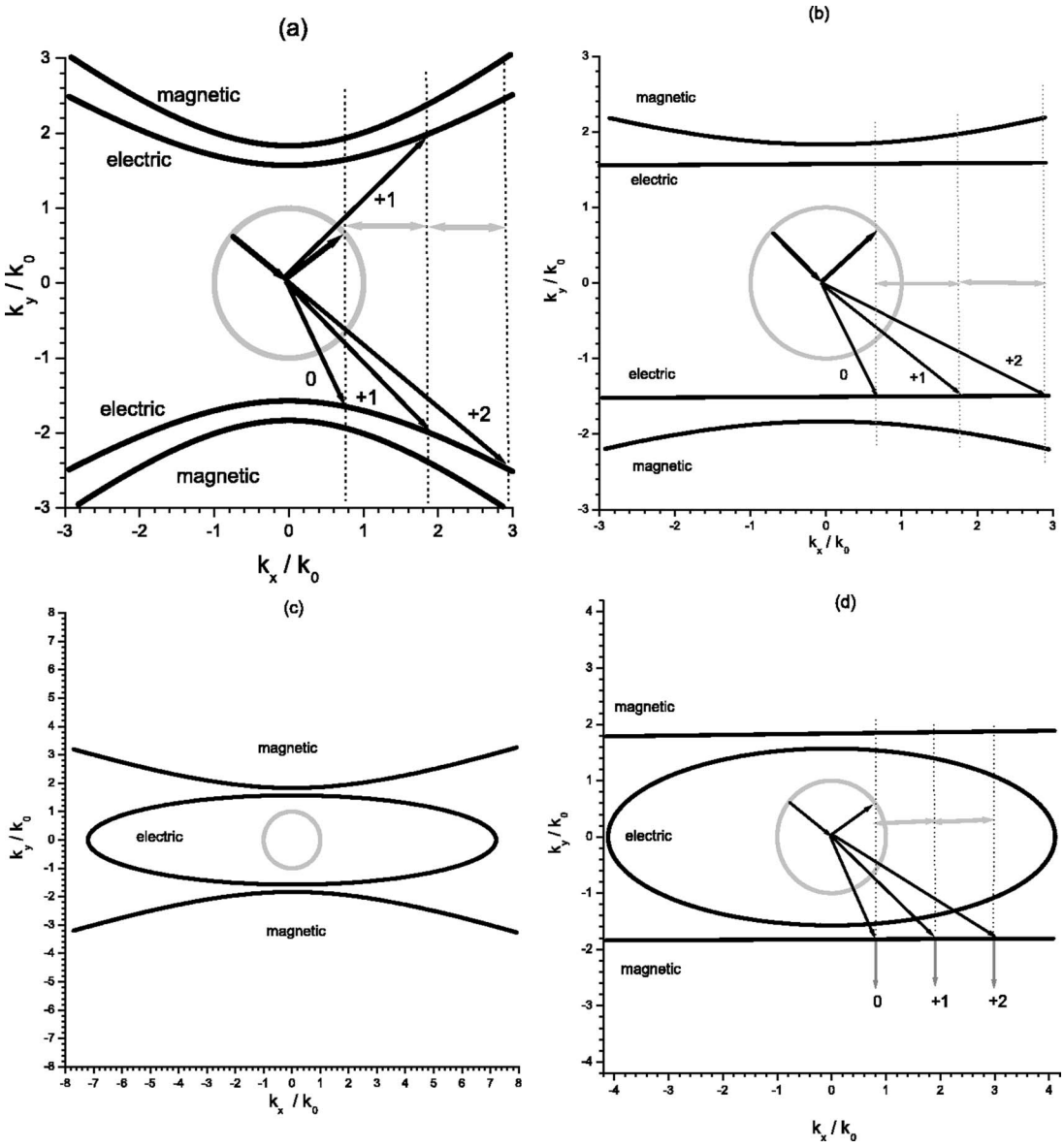

Fig. 5. Reciprocal space maps for cases IIA and IIB, when $\theta_c = \pi/2$ and $\lambda_0/d = 1.1$; $k_x = \vec{k} \cdot \hat{x}$ and $k_y = \vec{k} \cdot \hat{y}$. (a) $\phi_c = 30°$, (b) $\phi_c = 43.57°$, (c) $\phi_c = 45°$, and (d) $\phi_c = 47.97°$. The graphical construction to find the refracted Floquet harmonics is not shown in (c) for the sake of clarity.

tion procedure described in the previous paragraph, we see that an infinite number of wave vectors $\vec{k}_n^{(E,M)}$ with real-valued components can be obtained for cases IIA and IIB, whenever $0 < \phi_c < \phi_c^e$. A curious situation occurs when $\phi_c = \phi_c^e$ [Fig. 5(b)]: the dispersion equation for harmonics of the magnetic type is still hyperbolic, but the dispersion equation for harmonics of the electric type is linear, indicating that all $\beta_n^{(E)}$ are real valued and independent of n. We have again a situation with an infinite number of refracted harmonics of both electric and magnetic types, but now all the projections onto the xy plane of the rays associated with the harmonics of the electric type are aligned parallel to the $-y$ axis, independently of the angle of incidence θ_0.

When $\phi_c^e < \phi_c < \phi_c^m$ [Fig. 5(c)], the dispersion equation for refracted harmonics of the magnetic type is still hyperbolic, but the dispersion equation for the electric type is elliptic, indicating the existence of an infinite number of refracted wave vectors $\vec{k}_n^{(M)}$ but a finite number of transmitted wave vectors $\vec{k}_n^{(E)}$, with real-valued components.

When $\phi_c = \phi_c^m$ [Fig. 5(d)], the curves representing the dispersion equation for refracted harmonics of the electric type continue to be ellipses, but the curves representing the dispersion equation for the magnetic type become straight lines parallel to the x axis. In the same manner as for harmonics of the electric type when $\phi_c = \phi_c^e$, now all $\beta_n^{(M)}$ are real valued and independent of n. Thus, there is an infinite number of refraction channels of the magnetic type, with all the projections onto the xy plane of the refracted rays aligned parallel to the $-y$ axis regardless of the angle of incidence. These projections are indicated in Fig. 5(d) by gray arrows for harmonics of orders $n = 0$, 1, and 2.

When $\phi_c > \phi_c^m$, the dispersion equation for refracted harmonics of both electric and magnetic types are elliptic, thereby indicating the existence of a finite number of transmitted wave vectors $\vec{k}_n^{(E,M)}$ with real-valued components. This situation is the same as for natural crystals.

As has been already discussed elsewhere,[18] the main feature that appears in gratings with indefinite constitutive tensors is the possibility of an infinite number of propagating harmonics refracting into the anisotropic diffracting medium. As computer implementations of the theoretical methods developed for conventional gratings (including the present one) are based on a finite number of propagating harmonics, particular attention must be paid when they are applied to the study of the new kind of grating. In situations in which the polarization state does not alter on diffraction, the Rayleigh and the differential methods have shown a lack of convergence,[18,24] due to the existence of an infinite number of propagating refracted Floquet harmonics.

Because of experience with gratings made of materials with indefinite constitutive tensors, we carefully examined the convergence of the numerical results obtained through the differential method reported here. For $h/d = 0.1$ and $\phi_c = 0°$, 15°, 30°, 43.57°, 45°, 47.97°, 60°, 75°, and 90°, we obtained good convergence and satisfaction of the principle of conservation of energy for all angles of incidence. The efficiency curves for specularly refracted Floquet harmonics of both the electric and the magnetic types and for *s*- and *p*-polarized incident waves for cases IIA and IIB are similar to those for case IN and are not shown. When the number of refracted propagating harmonics is finite (in our example when $\phi_c > \phi_c^m$, generally when $\phi_c > \max\{\phi_c^e, \phi_c^m\}$), we ascertained that good results are obtained with the differential method for $h/d \leq 3$[34]; however, when the number of refracted propagating harmonics is infinite, the differential method fails to give adequate results for $h/d > 0.2$.

B. Optic Axis in the *yz* Plane

Next, we consider the optic axis $\hat{c}$ lying in the *yz* plane. On setting $\phi_c = 90°$ in Eq. (2), for the refracted Floquet har-

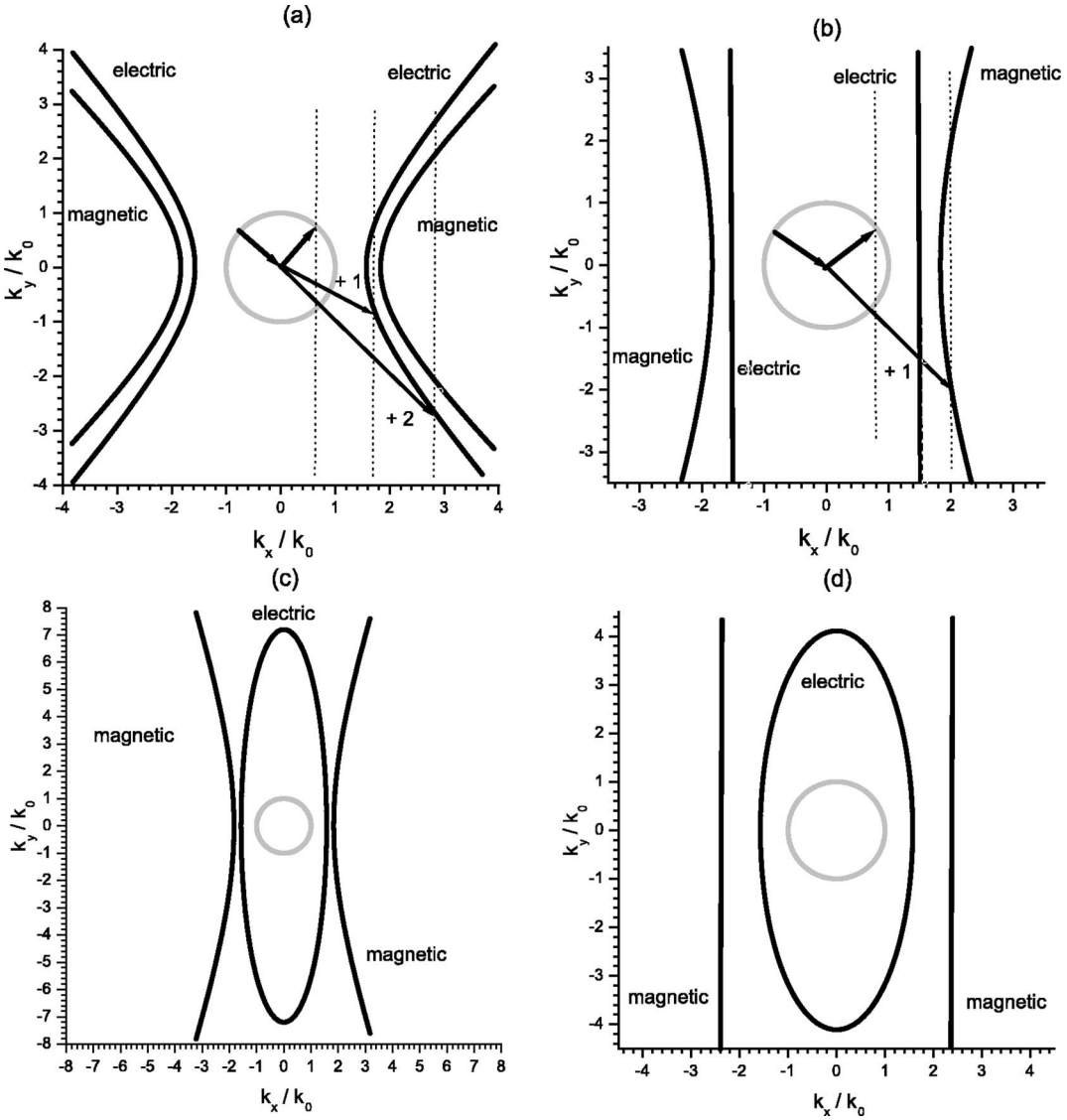

Fig. 6. Reciprocal space maps for cases IIA and IIB, when $\phi_c = 90°$ and $\lambda_0/d = 1.1$; $k_x = \vec{k} \cdot \hat{x}$ and $k_y = \vec{k} \cdot \hat{y}$. (a) $\theta_c = 15°$, (b) $\theta_c = 43.57°$, (c) $\theta_c = 45°$, and (d) $\theta_c = 47.97°$.

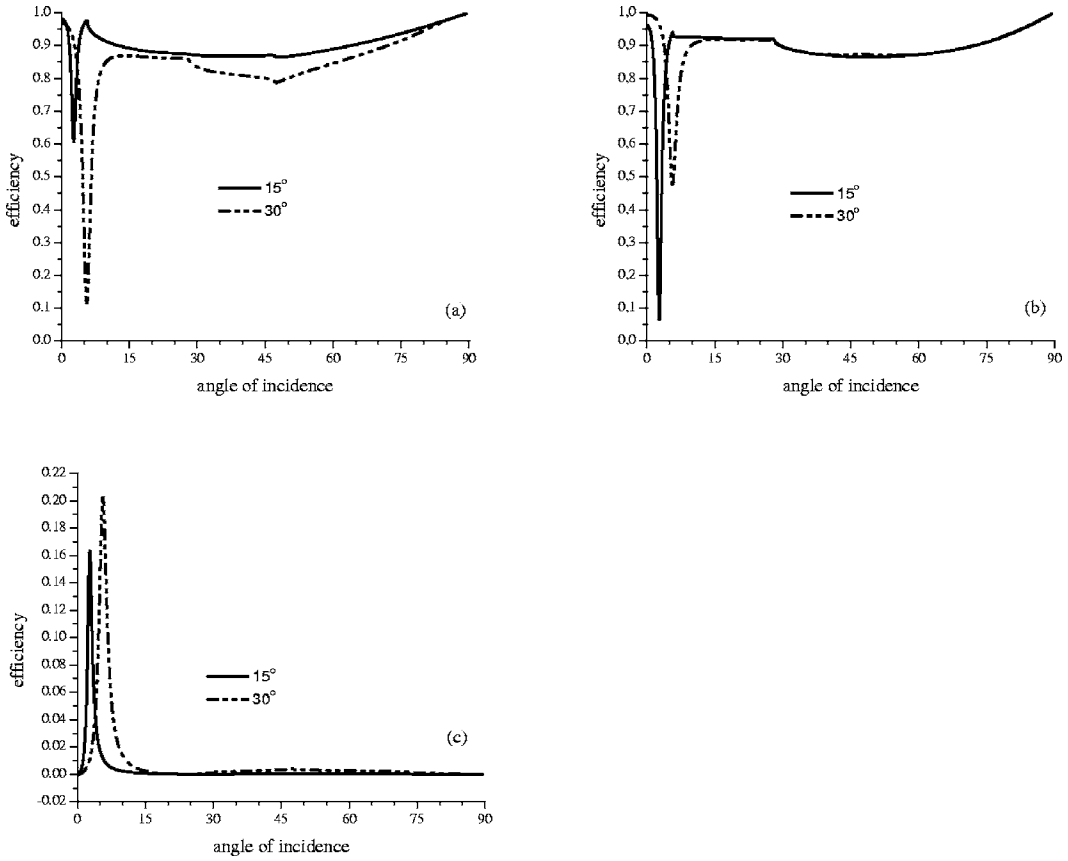

Fig. 7. Specular reflection efficiencies versus the angle of incidence θ_0 for a sinusoidal grating delineated by Eq. (29) with $h/d=0.1$ and illuminated from the vacuous region, when the constitutive scalars are chosen for case IIA, $\lambda_0=1.1d$, and $\phi_c=90°$. The values of θ_c are indicated on the plots. (a) ρ_0^{ss}, (b) ρ_0^{pp}, and (c) ρ_0^{sp}.

monics of the electric type Eq. (9) gives the dispersion equation

$$\alpha_n^2 + \left(\sin^2 \theta_c + \frac{\epsilon_\parallel}{\epsilon_\perp} \cos^2 \theta_c \right) (\beta_n^{(E)})^2 = k_0^2 \mu_\perp \epsilon_\parallel, \qquad (34)$$

whereas, for the refracted Floquet harmonics of the magnetic type, Eq. (10) gives the dispersion equation

$$\alpha_n^2 + \left(\sin^2 \theta_c + \frac{\mu_\parallel}{\mu_\perp} \cos^2 \theta_c \right) (\beta_n^{(M)})^2 = k_0^2 \epsilon_\perp \mu_\parallel. \qquad (35)$$

Taking into account that for cases IP and IN the dispersion equations are elliptic for all orientations of the optic axis and that the characteristics of elliptic dispersion equations have been extensively discussed for gratings made of natural crystals, we have elected here to not discuss those two cases.

Cases IIA and IIB, however, allow for new possibilities, e.g., an infinite number of refraction channels. Indeed, from Eqs. (34) and (35), we find again that dispersion equations for these two cases can be either elliptic or hyperbolic, depending on the orientation of the optic axis. Starting from $\theta_c=0°$, we can easily deduce the existence of critical angles for θ_c at which the dispersion curves change from hyperbolic to elliptic. For refracted harmonics of the electric type, this angle is

$$\theta_c^e = \tan^{-1}[(-\epsilon_\parallel/\epsilon_\perp)^{1/2}], \qquad (36)$$

whereas for refracted harmonics of the magnetic type the critical angle is given by

$$\theta_c^m = \tan^{-1}[(-\mu_\parallel/\mu_\perp)^{1/2}]. \qquad (37)$$

When $\theta_c=\theta_c^e$, the dispersion curves for refracted Floquet harmonics propagating in the xy plane are straight lines (electric type) and hyperbolas (magnetic type); however, for $\theta_c=\theta_c^m$, the dispersion curves are ellipses (electric type) and straight lines (magnetic type). Values of the critical angle for cases IIA and IIB are $\theta_c^e=43.57°$ and $\theta_c^m=47.97°$, respectively.

In Fig. 6, we have plotted the reciprocal space maps for cases IIA and IIB for four orientations of the optic axis: $\theta_c=15°$ (both dispersion curves are hyperbolic), $\theta_c=\theta_c^e=43.57°$ (electric type is linear and magnetic type is hyperbolic), $\theta_c=45°$ (electric type is elliptic and magnetic type is hyperbolic), and $\theta_c=\theta_c^m=47.97°$ (electric type is elliptic and magnetic type is linear). For $\theta_c>\theta_c^m=47.97°$, the refracted Floquet harmonics of both types have elliptic dispersion relations (not shown).

From the graphical constructions shown in Fig. 6 we find that—just as in Subsection 4.A—an infinite number of Floquet harmonics can be propagated into the diffracting medium. However, there are some differences between $\hat{c}\cdot\hat{y}=0$ and $\hat{c}\cdot\hat{x}=0$ that lead to three rather curious consequences:

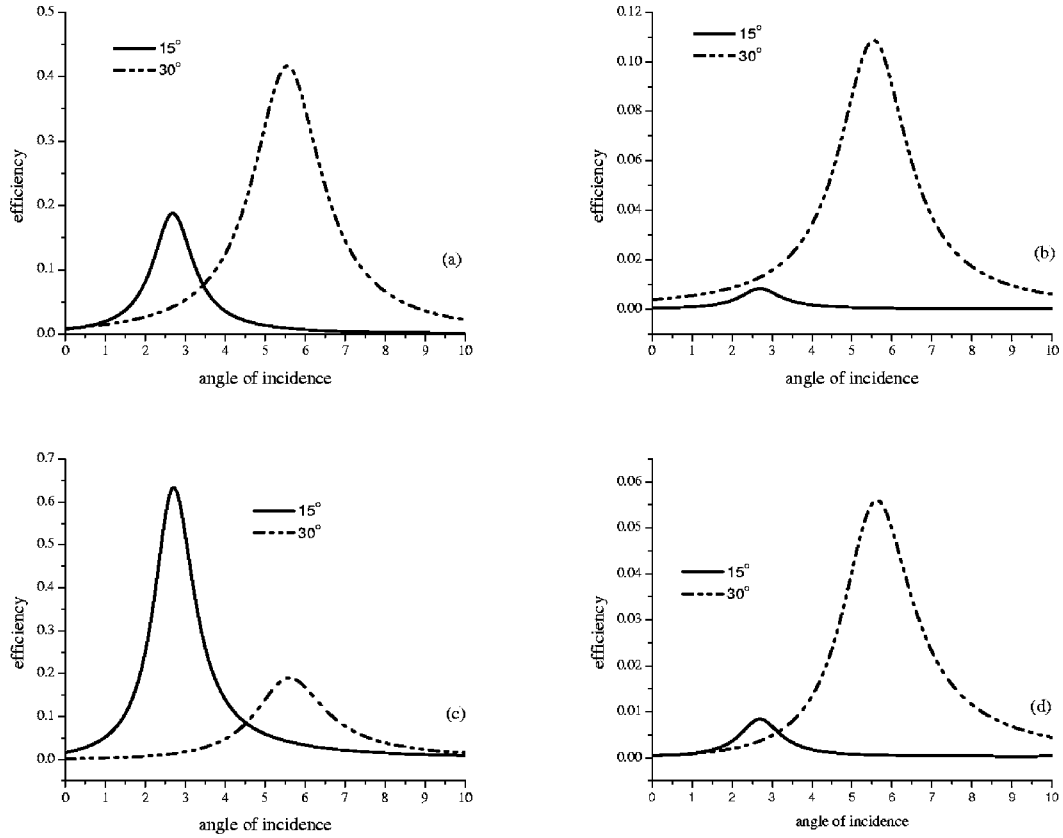

Fig. 8. Nonspecular refraction efficiencies versus the angle of incidence θ_0 for a sinusoidal grating delineated by Eq. (29) with $h/d=0.1$ illuminated from the vacuous region, when the constitutive scalars are chosen for case IIA, $\lambda_0=1.1d$, and $\phi_c=90°$. The values of θ_c are indicated on the plots. (a) τ_2^{Es}, (b) τ_2^{Ms}, (c) τ_2^{Ep}, and (d) τ_2^{Mp}.

- First, the specularly refracted harmonics of both types are not allowed to propagate when $\hat{c}\cdot\hat{x}=0$, but that restriction does not exist when $\hat{c}\cdot\hat{y}=0$.
- Second, it is possible that low-order ($|n|$ small) refracted harmonics are not allowed to propagate when $\hat{c}\cdot\hat{x}=0$, depending on the value of λ_0/d, but that restriction does not exist when $\hat{c}\cdot\hat{y}=0$. For instance, when $\lambda_0/d=1.1$, this distinction is shown by the refracted harmonics of order $n=-1$.
- Third, whereas for $\hat{c}\cdot\hat{x}=0$ the straight-line dispersion curves corresponding to the critical angles ϕ_c^e and ϕ_c^m are parallel to the x axis, leading to an infinite number of refracted harmonics, for $\hat{c}\cdot\hat{x}=0$ the straight-line dispersion curves corresponding to the critical angles θ_c^e and θ_c^m are parallel to the y axis and thus are not associated with an infinite number of refracted harmonics. Furthermore, for $\hat{c}\cdot\hat{x}=0$ the refracted harmonics of the electric type associated with the linear dispersion curves can be excited only for those angles of incidence θ_0 that satisfy the relation

$$\sin\theta_0=\sqrt{\mu_\perp\epsilon_\parallel}\pm n\frac{\lambda_0}{d}, \tag{38}$$

whereas refracted harmonics of the magnetic type associated with the linear dispersion curves can be excited only if

$$\sin\theta_0=\sqrt{\epsilon_\perp\mu_\parallel}\pm n\frac{\lambda_0}{d}, \tag{39}$$

with n as an integer. When these conditions apply, the projections onto the xy plane of the rays associated with the linear dispersion curves are parallel to the x axis, regardless of θ_0. We note that in these curious situations, currently under investigation, no power can be coupled into the diffracting medium through these channels.

Let us now turn to the diffraction efficiencies when the grating profile is the sinusoid [Eq. (29)]. Specular reflection efficiencies for case IIA are plotted as functions of θ_0 in Fig. 7, for $\theta_c=15°$ and $\theta_c=30°$. For both orientations of the optic axis, the dispersion equations for the refracted harmonics are hyperbolic. The plots show that the copolarized specularly reflected harmonics carry almost all the energy incident on the grating for all angles of incidence, except at certain values of θ_0 where sharp dips are observed. At these angles, the specular cross-polarized reflection also exhibits peaks, reaching ≈0.16 for $\theta_c=15°$ and ≈0.2 for $\theta_c=30°$.

Although the specularly refracted harmonics are evanescent, a strong coupling with refracted harmonics of higher orders is observed, as we show in Fig. 8, where the efficiencies of the refracted harmonic $n=2$ of both types are plotted for both polarization states of the incident plane wave for $0°<\theta_0<10°$. The peaks are associated

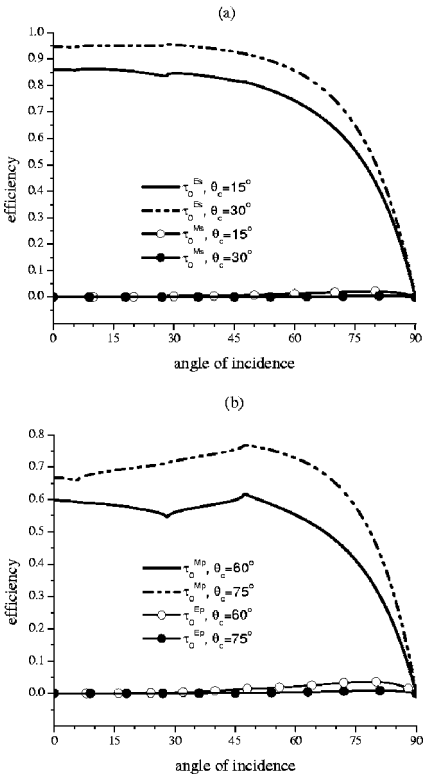

Fig. 9. Specular refraction efficiencies versus the angle of incidence θ_0 for a sinusoidal grating delineated by Eq. (29) with $h/d=0.1$ and illuminated from the vacuous region, when the constitutive scalars are chosen for case IIA, $\lambda_0=1.1d$, and $\phi_c=90°$. The values of θ_c are indicated on the plots. Incident polarization state: (a) s, (b) p.

with the excitation of surface plasmons at the periodic boundary.[17,18] One can approximately obtain the position of the peaks by taking the real part of the zero of the characteristic determinant of the system of linear equations for the diffraction amplitudes.

Next, we consider two other orientations of the optic axis: $\theta_c=60°$ and $\theta_c=75°$. The dispersion curves for the refracted Floquet harmonics of the electric and the magnetic types are elliptic, resembling the IP and IN cases. Specular refraction efficiencies for case IIA are plotted in Fig. 9, for both polarization states of the incident plane wave. When the incident polarization state is s (p), the specularly refracted harmonic of the magnetic (electric) type is weak in the plots presented.

The foregoing observation may be explained as follows. When the optic axis is oriented along the z axis (i.e., $\theta_c=90°$), no polarization conversion takes place owing to diffraction, and the full boundary-value problem can be separated into two smaller problems for autonomous linear polarization states[18]; the refracted harmonics of the electric type have the s-polarization state, whereas those of the magnetic type are p polarized. Although we are not considering exactly this case, as $\theta_c \to 90°$, it seems reasonable to obtain that tendency in our results. For a p-polarized incident plane wave, there is a coupling of energy into the $n=-1$ refracted harmonic of the magnetic type, which reaches a value of ≈ 0.22 at $\theta_0 \approx 22°$ (not shown). The increased coupling into higher-order refracted harmonics was also observed in gratings with constitutive parameters of case IN and is an important difference between materials with negative definite tensors or indefinite tensors and conventional materials with positive definite tensors.

For orientations of the optic axis in θ_c regimes near $\theta_c^{e,m}$, the numerical implementation of the differential method becomes unstable, and results do not converge. The problem near these singularities, currently under investigation, is not totally understood, but it seems to be related to the fact that power fluxes associated with rather vertical branches of the dispersion curves are almost parallel to the x axis. Therefore, owing to the existence of numerical errors, great care must be taken to select those solutions of Eqs. (34) and (35) that satisfy the radiation condition.

C. Deep Sinusoidal Gratings

The gratings studied in Subsections 4.A and 4.B are not deep because $h/d=0.1$. Let us therefore turn to deep gratings for which computational methods are often troublesome.[12,18,24] Sample results are presented for constitutive scalar sets belonging to case IIA and for $\lambda_0/d=1.1$. We consider here two orientations of the optic axis: one leading to elliptic and the other to hyperbolic dispersion curves.

Tables 1 and 2 show the computed reflection and refraction efficiencies for sinusoidal gratings with different values of h/d, for normally incident plane waves that are s

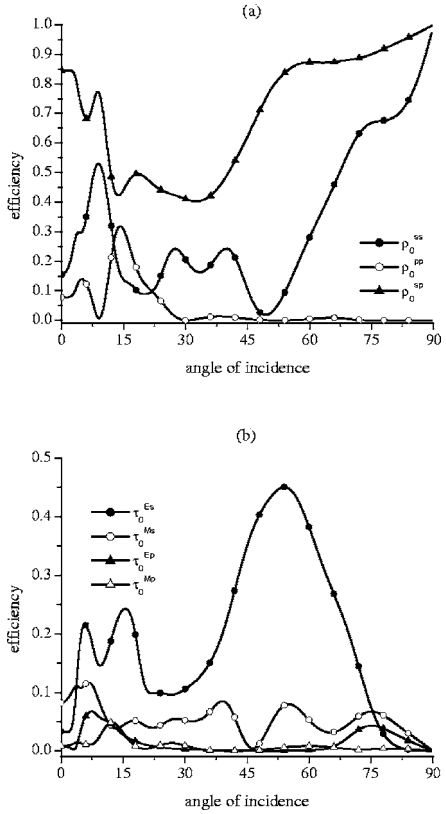

Fig. 10. Specular reflection and refraction efficiencies versus the angle of incidence θ_0 for a sinusoidal grating delineated by Eq. (29) and illuminated from the vacuous region, when the constitutive scalars are chosen for case IIA, $\lambda_0=1.1d$, $h/d=3.0$, $\theta_c=90°$, and $\phi_c=60°$. (a) $\rho_0^{ss,pp,sp}$, (b) $\tau_0^{Es,Ms,Ep,Mp}$.

Table 1. Diffraction Efficiencies Computed for Sinusoidal Gratings Delineated by Eq. (29)[a]

	$h/d=0.8$	$h/d=1.4$	$h/d=1.8$	$h/d=2.2$	$h/d=3.0$
ρ_0^{ss}	0.1009×10^{-1}	0.1617	0.2087	0.3462	0.1552
τ_0^{Es}	0.9989×10^{-1}	0.1729	0.2897	0.2938	0.3367×10^{-1}
τ_0^{Ms}	0.4802×10^{-2}	0.7171×10^{-1}	0.1331	0.5626×10^{-1}	0.8214×10^{-1}
τ_{-1}^{Es}	0.3288	0.1950	0.5198×10^{-1}	0.5789×10^{-1}	0.3162
τ_{-1}^{Ms}	0.2891×10^{-1}	0.5541×10^{-1}	0.1796×10^{-1}	0.5239×10^{-1}	0.8214×10^{-2}
PC	1.00000	1.00000	1.00000	1.00000	1.00003

[a]Gratings have different values of h/d and are illuminated from the vacuous region by an *s*-polarized plane wave, when the constitutive scalars are chosen for case IIa, $\lambda_0=1.1d$, $\theta_c=90°$, $\phi_c=60°$, and $\theta_0=0°$. The differential method was used with $|n|\leqslant 43$. PC, principle of conservation.

Table 2. Same as Table 1 but for an Incident *p*-Polarized Plane Wave

	$h/d=0.8$	$h/d=1.4$	$h/d=1.8$	$h/d=2.2$	$h/d=3.0$
ρ_0^{pp}	0.5117×10^{-1}	0.4518	0.3199	0.5955	0.8451
τ_0^{Ep}	0.5353	0.1333	0.1489×10^{-1}	0.2173×10^{-1}	0.8824×10^{-2}
τ_0^{Mp}	0.4526×10^{-1}	0.2425×10^{-1}	0.4050×10^{-1}	0.2934×10^{-1}	0.8662×10^{-2}
τ_{-1}^{Ep}	0.4941×10^{-1}	0.1553	0.1789	0.1389	0.2888×10^{-1}
τ_{-1}^{Mp}	0.6664×10^{-1}	0.6146×10^{-2}	0.1911×10^{-1}	0.1153×10^{-2}	0.7546×10^{-3}
PC	1.00000	1.00000	1.00000	1.00000	1.00002

and *p* polarized, respectively. The chosen orientation of the optic axis ($\theta_c=90°$ and $\phi_c=60°$) is such that the dispersion curves for refracted harmonics of both types are elliptic; hence, the number of refraction channels is finite. The quantity indicated as PC in both tables should equal unity, if the principle of conservation of energy is satisfied. We used Floquet harmonics of orders $|n|\leqslant 35$ for $0.8\leqslant h/d\leqslant 2.2$ and $|n|\leqslant 43$ for $h/d=3$, which sufficed to ensure that the principle of conservation of energy was satisfied to an error of 1 part per million. As can be deduced from these tables, the differential method performs well for deep gratings with $h/d\leqslant 3.0$.[34]

Figure 10 contains plots of the specular diffraction efficiencies as functions of θ_0 for the same parameters as in Tables 1 and 2 except that $h/d=3.0$. The specular copolarized as well as the cross-polarized reflection efficiencies fluctuate quite significantly as the angle of incidence is changed. In particular, ρ_0^{pp} equals 0.85 for normal incidence and exceeds 0.4 for all θ_0. In contrast, ρ_0^{ss} fluctuates less and peaks at 0.53 when $\theta_0\approx 9°$. Of course, both efficiencies tend to unity as $\theta_0\to 90°$. The efficiency of polarization conversion ρ_0^{sp} is low, with a maximum value of 0.32 when $\theta_0\approx 14°$. The specular transmission efficiencies in Fig. 10(b) are small—except for τ_0^{Es}, which is low at normal incidence, but then increases, with a maximum value of approximately 0.45 at $\theta_0\approx 54°$.

Elsewhere[18,24] we have shown that, in situations for which scalar analysis suffices and a full-vector analysis is unnecessary, both the Rayleigh method and the differential method yield nonconvergent results for gratings made of materials characterized by indefinite constitutive tensors. The lack of convergence was attributed to the existence of an infinite number of propagating harmonics refracted into the grating medium. For further investigation of this point, to provide our final example in this paper, we reoriented the optic axis to $\phi_c=30°$, the other parameters remaining the same as for Tables 1 and 2. Physically, this situation is completely different, however, since an infinite number of refracted Floquet harmonics are allowed now to propagate. In Tables 3 and 4, we present some diffraction efficiencies for different values of h/d. These tables show that the differential method give adequate results for shallow gratings with $h/d\leqslant 0.2$, for which the efficiencies converge satisfactorily. For values of $h/d>0.2$, the method becomes unstable, and the computed results do not satisfy the principle of conservation of energy. This observation is not surprising, and it supports the connection between the lack of convergence and the existence of an infinite number of refraction channels in the diffracting medium.

5. CONCLUDING REMARKS

We applied the differential method to examine the diffraction of linearly polarized plane waves due to the periodically corrugated boundary of vacuum and a linear, homogeneous, nondissipative, uniaxial dielectric–magnetic material. We specifically considered two classes of diffracting materials: those with negative definite permittivity and permeability tensors and those with indefinite permittivity and permeability tensors. The dispersion equations turn out to be elliptic for the first class of diffracting materials. For the second class of diffracting materials, the dispersion equations can be hyperbolic, elliptic, or linear, depending on the orientation of the optic axis. When the dispersion equations are elliptic, a finite number of refraction channels are supported, just as for gratings made of PPV materials.

We demonstrated with the aid of several examples that hyperbolic or linear dispersion equations imply the possibility of an infinite number of refraction channels. This fact leads to difficulties with the differential method, par-

Table 3. Same as Table 1 but for $\phi_c = 30°$[a]

	$h/d=0.1$	$h/d=0.15$	$h/d=0.2$
ρ_0^{ss}	0.3362×10^{-2}	0.1436×10^{-2}	0.1508×10^{-3}
τ_0^{Es}	0.2410	0.2337	0.2255
τ_0^{Ms}	0.5794	0.4165	0.2547
τ_{-1}^{Es}	0.5070×10^{-2}	0.1022×10^{-1}	0.1594×10^{-1}
τ_{-1}^{Ms}	0.7738×10^{-1}	0.1396	0.1808
PC	1.00000	1.00000	1.00006

[a]The differential method was used with $|n|\leqslant 35$. Note that convergent results were not obtained for $h/d>0.2$.

ticularly as the corrugations deepen, and nonconvergent as well as unphysical results are obtained. Thus the emergence of NPV materials has helped us comprehensively identify a new research frontier in grating theory.

APPENDIX A

The matrix e in Eq. (17) is defined as

$$\mathsf{e}=\begin{bmatrix} \left[\!\left[\frac{1}{\bar{\epsilon}^{11}}\right]\!\right]^{-1} & \left[\!\left[\frac{1}{\bar{\epsilon}^{11}}\right]\!\right]^{-1}\left[\!\left[\frac{\epsilon^{12}}{\bar{\epsilon}^{11}}\right]\!\right] & \left[\!\left[\frac{1}{\bar{\epsilon}^{11}}\right]\!\right]^{-1}\left[\!\left[\frac{\bar{\epsilon}^{13}}{\bar{\epsilon}^{11}}\right]\!\right] \\ \left[\!\left[\frac{\epsilon^{21}}{\bar{\epsilon}^{11}}\right]\!\right]\left[\!\left[\frac{1}{\bar{\epsilon}^{11}}\right]\!\right]^{-1} & \left[\!\left[\frac{\epsilon^{21}}{\bar{\epsilon}^{11}}\right]\!\right]\left[\!\left[\frac{1}{\bar{\epsilon}^{11}}\right]\!\right]^{-1}\left[\!\left[\frac{\epsilon^{12}}{\bar{\epsilon}^{11}}\right]\!\right]+\left[\!\left[\bar{\epsilon}^{22}-\frac{\bar{\epsilon}^{21}\bar{\epsilon}^{12}}{\bar{\epsilon}^{11}}\right]\!\right] & \left[\!\left[\frac{\epsilon^{21}}{\bar{\epsilon}^{11}}\right]\!\right]\left[\!\left[\frac{1}{\bar{\epsilon}^{11}}\right]\!\right]^{-1}\left[\!\left[\frac{\bar{\epsilon}^{13}}{\bar{\epsilon}^{11}}\right]\!\right]+\left[\!\left[\bar{\epsilon}^{23}-\frac{\bar{\epsilon}^{21}\bar{\epsilon}^{13}}{\bar{\epsilon}^{11}}\right]\!\right] \\ \left[\!\left[\frac{\bar{\epsilon}^{31}}{\bar{\epsilon}^{11}}\right]\!\right]\left[\!\left[\frac{1}{\bar{\epsilon}^{11}}\right]\!\right]^{-1} & \left[\!\left[\frac{\bar{\epsilon}^{31}}{\bar{\epsilon}^{11}}\right]\!\right]\left[\!\left[\frac{1}{\bar{\epsilon}^{11}}\right]\!\right]^{-1}\left[\!\left[\frac{\epsilon^{12}}{\bar{\epsilon}^{11}}\right]\!\right]+\left[\!\left[\bar{\epsilon}^{32}-\frac{\bar{\epsilon}^{31}\bar{\epsilon}^{12}}{\bar{\epsilon}^{11}}\right]\!\right] & \left[\!\left[\frac{\bar{\epsilon}^{31}}{\bar{\epsilon}^{11}}\right]\!\right]\left[\!\left[\frac{1}{\bar{\epsilon}^{11}}\right]\!\right]^{-1}\left[\!\left[\frac{\bar{\epsilon}^{13}}{\bar{\epsilon}^{11}}\right]\!\right]+\left[\!\left[\bar{\epsilon}^{33}-\frac{\bar{\epsilon}^{31}\bar{\epsilon}^{13}}{\bar{\epsilon}^{11}}\right]\!\right] \end{bmatrix}, \tag{A1}$$

where $[\![f]\!]$ stands for the Toeplitz matrix generated by the Fourier coefficients of a periodic function f, such that $[\![f]\!]_{mn}=f_{m-n}$ and $\bar{\epsilon}^{\rho\sigma}$ are components of $\bar{\epsilon}$ in system $O\bar{x}^1\bar{x}^2\bar{x}^3$. One obtains the matrix m in Eq. (18) from Eq. (A1) after replacing ϵ with μ. The G matrix used in Eqs. (19) and (20) is given by

$$G=\sec^2\zeta\begin{bmatrix} 1 & -([\![\dot{a}]\!]+\sin\zeta) & 0 \\ -([\![\dot{a}]\!]+\sin\zeta) & \cos^2\zeta+([\![\dot{a}]\!]+\sin\zeta)^2 & 0 \\ 0 & 0 & \cos^2\zeta \end{bmatrix}, \tag{A2}$$

where $\dot{a}=\mathrm{d}a/\mathrm{d}x^1$.

APPENDIX B

The expressions of matrices Z are given in expressions (18) and (20) of Ref. 20:

$$Z_{11}=\mathsf{e}^{11}-\mathsf{e}^{12}(\mathsf{e}^{22})^{-1}\mathsf{e}^{21},\qquad Z_{12}=\mathsf{e}^{12}(\mathsf{e}^{22})^{-1},$$

$$Z_{13}=\mathsf{e}^{13}-\mathsf{e}^{12}(\mathsf{e}^{22})^{-1}\mathsf{e}^{23},$$

$$Z_{21}=(\mathsf{e}^{22})^{-1}\mathsf{e}^{21},\qquad Z_{22}=\frac{1}{\kappa_0}(\mathsf{e}^{22})^{-1},$$

$$Z_{23}=(\mathsf{e}^{22})^{-1}\mathsf{e}^{23},$$

$$Z_{31}=\mathsf{e}^{31}-\mathsf{e}^{32}(\mathsf{e}^{22})^{-1}\mathsf{e}^{21},\qquad Z_{32}=\mathsf{e}^{32}(\mathsf{e}^{22})^{-1}, \tag{B1}$$

Table 4. Same as Table 3 but for an Incident *p*-Polarized Plane Wave

	$h/d=0.1$	$h/d=0.15$	$h/d=0.2$
ρ_0^{pp}	0.4948×10^{-2}	0.2465×10^{-2}	0.5204×10^{-3}
τ_0^{Ep}	0.7408	0.7358	0.7256
τ_0^{Mp}	0.1798	0.1147	0.5440×10^{-1}
τ_{-1}^{Ep}	0.1519×10^{-2}	0.3617×10^{-2}	0.7302×10^{-2}
τ_{-1}^{Mp}	0.3264×10^{-1}	0.5712×10^{-1}	0.6991×10^{-1}
PC	1.00000	1.00000	1.00005

$$Z_{33}=\mathsf{e}^{33}-\mathsf{e}^{32}(\mathsf{e}^{22})^{-1}\mathsf{e}^{23}.$$

Expressions of matrices T are obtained from Eqs. (B1) on replacing e by m.

ACKNOWLEDGMENTS

R. A. Depine and M. E. Inchaussandague acknowledge financial support from Consejo Nacional de Investigaciones Científicas y Técnicas, Agencia Nacional de Promoción Científica y Tecnológica (ANPCYT-BID 1201/OC-AR-PICT14099), and Universidad de Buenos Aires. A. Lakhtakia thanks the National Science Foundation-funded Center for the Integration of Research, Teaching, and Learning Project for partial support. Corresponding author M. E. Inchaussandague can be reached by e-mail at mei@df.uba.ar. R. A. Depine's e-mail address is rdep@df.uba.ar, and A. Lakhtakia's e-mail address is akhlesh@psu.edu.

REFERENCES AND NOTES

1. A. Lakhtakia, M. W. McCall, and W. S. Weiglhofer, "Negative phase-velocity mediums," in W. S. Weiglhofer and A. Lakhtakia, eds., *Introduction to Complex Mediums for Optics and Electromagnetics* (SPIE, 2003).
2. J. B. Pendry, "Negative refraction," Contemp. Phys. **45**, 191–202 (2004).
3. S. A. Ramakrishna, "Physics of negative refractive index materials," Rep. Prog. Phys. **68**, 449–521 (2005).
4. M. W. McCall, A. Lakhtakia, and W. S. Weiglhofer, "The negative index of refraction demystified," Eur. J. Phys. **23**, 353–359 (2002).
5. A. D. Boardman, N. King, and L. Velasco, "Negative refraction in perspective," Electromagnetics **25**, 365–389 (2005).
6. T. G. Mackay and A. Lakhtakia, "Plane waves with negative phase velocity in Faraday chiral mediums," Phys. Rev. E **69**, 026602 (2004).
7. C. G. Parazzoli, R. B. Greegor, L. Li, B. E. C. Koltenbah, and M. Tanielian, "Experimental verification and simulation of negative index of refraction using Snell's law," Phys. Rev. Lett. **90**, 107401 (2003).
8. L. B. Hu and S. T. Chui, "Characteristics of electromagnetic wave propagation in uniaxially anisotropic left-handed materials," Phys. Rev. B **66**, 085108 (2002).
9. A. Lakhtakia and J. A. Sherwin, "Orthorhombic materials and perfect lenses," Int. J. Infrared Millim. Waves **24**, 19–23 (2003).
10. D. R. Smith and D. Schurig, "Electromagnetic wave propagation in media with indefinite permittivity and permeability tensors," Phys. Rev. Lett. **90**, 077405 (2003).
11. D. R. Smith, P. Kolinko, and D. Schurig, "Negative refraction in indefinite media," J. Opt. Soc. Am. B **21**, 1032–1043 (2004).
12. D. Maystre, ed., *Selected Papers on Diffraction Gratings* (SPIE, 1993).
13. R. A. Depine and A. Lakhtakia, "Plane-wave diffraction at the periodically corrugated boundary of vacuum and a negative-phase-velocity material," Phys. Rev. E **69**, 057602 (2004).
14. R. A. Depine and A. Lakhtakia, "Perturbative approach for diffraction due to a periodically corrugated boundary between vacuum and a negative phase-velocity material," Opt. Commun. **233**, 277–282 (2004).
15. R. A. Depine and A. Lakhtakia, "Diffraction gratings of isotropic negative phase-velocity materials," Optik **116**, 31–43 (2005).
16. D. R. Smith, P. M. Rye, J. J. Mock, D. C. Vier, and A. F. Starr, "Enhanced diffraction from a grating on the surface of a negative-index metamaterial," Phys. Rev. Lett. **93**, 137405 (2004).
17. R. A. Depine, A. Lakhtakia, and D. R. Smith, "Enhanced diffraction by a rectangular grating made of a negative phase-velocity (or negative index) material," Phys. Rev. A **337**, 155–160 (2005).
18. R. A. Depine and A. Lakhtakia, "Diffraction by a grating made of an uniaxial dielectric–magnetic medium exhibiting negative refraction," New J. Phys. **7**, 158 (2005).
19. J. Chandezon, M. Dupuis, G. Cornet, and D. Maystre, "Multicoated gratings: a differential formalism applicable in the entire optical region," J. Opt. Soc. Am. **72**, 839–846 (1982).
20. L. Li, "Oblique-coordinate-system-based Chandezon method for modeling one-dimensionally periodic, multilayer, inhomogeneous, anisotropic gratings," J. Opt. Soc. Am. A **16**, 2521–2531 (1999).
21. L. Li, J. Chandezon, G. Granet, and J. P. Plumey, "Rigorous and efficient grating-analysis method made easy for optical engineers," Appl. Opt. **38**, 304–313 (1999).
22. M. E. Inchaussandague and R. A. Depine, "Polarization conversion from diffraction gratings made of uniaxial crystals," Phys. Rev. E **54**, 2899–2911 (1996).
23. M. E. Inchaussandague and R. A. Depine, "Rigorous vector theory for diffraction gratings made of biaxial crystals," J. Mod. Opt. **44**, 1–27 (1997).
24. R. A. Depine, M. E. Inchaussandague, and A. Lakhtakia, "Application of the differential method to uniaxial gratings with an infinite number of refraction channels: scalar case," Opt. Commun. **258**, 90–96 (2006).
25. A. Lakhtakia, V. K. Varadan, and V. V. Varadan, "Plane waves and canonical sources in a gyroelectromagnetic uniaxial medium," Int. J. Electron. **71**, 853–861 (1991).
26. A. Lakhtakia, V. K. Varadan, and V. V. Varadan, "Reflection and transmission of plane waves at the planar interface of a general uniaxial medium and free space," J. Mod. Opt. **38**, 649–657 (1991).
27. R. A. Depine, M. E. Inchaussandague, and A. Lakhtakia, "Classification of dispersion equations for homogeneous dielectric–magnetic uniaxial materials," J. Opt. Soc. Am. A (to be published).
28. H. Lütkepohl, *Handbook of Matrices* (Wiley, 1996).
29. H. C. Chen, *Theory of Electromagnetic Waves: A Coordinate-Free Approach* (McGraw-Hill, 1983).
30. M. N. L. Narasimhan, *Principles of Continuum Mechanics* (Wiley, 1993).
31. The term diffraction efficiency encompasses both reflection efficiency and refraction efficiency.
32. A. Lakhtakia, "On planewave remittances and Goos–Hänchen shifts of planar slabs with negative real permittivity and permeability," Electromagnetics **23**, 71–75 (2003).
33. A. Lakhtakia and M. W. McCall, "Counterposed phase velocity and energy-transport velocity vectors in a dielectric–magnetic uniaxial medium," Optik (Stuttgart) **115**, 28–30 (2004).
34. Our limited computational resources did not allow us to check for $h/d > 3.0$.